Excitation Energy Transfer and Trapping in Higher Plant Photosystem II Complexes with Different Antenna Sizes

Caffarri, Stefano; Broess, Koen; Croce, Roberta; van Amerongen, Herbert; Brown, Leonid S.

Published in:
Biophysical Journal

DOI:
10.1016/j.bpj.2011.03.049

Publication date:
2011

Excitation Energy Transfer and Trapping in Higher Plant Photosystem II Complexes with Different Antenna Sizes

Stefano Caffarri,[†‡§*] Koen Broess,[¶] Roberta Croce,[**] and Herbert van Amerongen[¶‖*]

[†]Aix Marseille Université, Laboratoire de Génétique et Biophysique des Plantes, Marseille, France; [‡]CEA, DSV, iBEB, Marseille, France; [§]CNRS, UMR6191 Biologie Végétale et Microbiologie Environnementales, Marseille, France; [¶]Wageningen University, Laboratory of Biophysics and [‖]Microspectroscopy Center, Wageningen, The Netherlands; and **Groningen University, Groningen Biomolecular Sciences and Biotechnology Institute, Department of Biophysical Chemistry, Groningen, The Netherlands

ABSTRACT We performed picosecond fluorescence measurements on well-defined Photosystem II (PSII) supercomplexes from *Arabidopsis* with largely varying antenna sizes. The average excited-state lifetime ranged from 109 ps for PSII core to 158 ps for the largest $C_2S_2M_2$ complex in 0.01% α-DM. Excitation energy transfer and trapping were investigated by coarse-grained modeling of the fluorescence kinetics. The results reveal a large drop in free energy upon charge separation (>700 cm^{-1}) and a slow relaxation of the radical pair to an irreversible state (~150 ps). Somewhat unexpectedly, we had to reduce the energy-transfer and charge-separation rates in complexes with decreasing size to obtain optimal fits. This strongly suggests that the antenna system is important for plant PSII integrity and functionality, which is supported by biochemical results. Furthermore, we used the coarse-grained model to investigate several aspects of PSII functioning. The excitation trapping time appears to be independent of the presence/absence of most of the individual contacts between light-harvesting complexes in PSII supercomplexes, demonstrating the robustness of the light-harvesting process. We conclude that the efficiency of the nonphotochemical quenching process is hardly dependent on the exact location of a quencher within the supercomplexes.

INTRODUCTION

Photosystem II (PSII) is a water-plastoquinone oxydoreductase embedded in the thylakoid membrane of plants, algae, and cyanobacteria. In higher plants, PSII is present mainly as dimers, and each monomer consists of at least 27–28 subunits, many of which coordinate chlorophylls (Chls) and carotenoids (1,2). PSII can be divided into two moieties: the core complex and the outer antenna system.

The crystal structure of the cyanobacterial core shows the presence of 35 Chl *a* molecules, two pheophytins *a*, and 12 β-carotene molecules (3). These pigments are associated to several proteins: 1), D1 and D2 complexes that, together with cytb559, constitute the reaction center (RC), coordinate the primary electron donor P680 and all cofactors of the electron transport chain; 2), CP47 and CP43, which coordinate Chl *a* and β-carotene molecules and act as an inner antenna; and 3), several low-molecular-weight subunits whose roles are not fully understood (4). The peripheral antenna system of plants and green algae is composed of members of the light-harvesting complex (LHC) multigenic family (5). The major antenna complex, LHCII, is composed of the products of genes Lhcb1–3 (6). It is organized in trimers and coordinates eight Chl *a*, six Chl *b*, and four xanthophyll molecules per monomeric subunit (7). Three more so-called minor complexes—CP29 (Lhcb4), CP26 (Lhcb5), and CP24 (Lhcb6)—are present as monomers in the membrane and coordinate 8, 9, and 10 Chls, respectively, and 2–3 xanthophylls (8). All of these complexes are involved in light absorption, transfer of excitation energy to the RC, and regulation of the excitation density (1,9). The number of these complexes in the membrane is variable and depends on the growing conditions (10).

Although PSII is a key component of the thylakoid membrane, information about its structure and functioning in higher plants is still limited due to the difficulty of purifying these complexes to homogeneity. Knowledge about the supramolecular organization of the complex has been obtained by electron microscopy and single-particle image averaging analysis on heterogeneous preparations obtained from mildly solubilized membranes in combination with biochemical analysis (11,12). It has been shown that the largest stable supercomplex of *Arabidopsis thaliana* is composed of a dimeric core (C_2); two trimeric LHCIIs (trimer S, where S means strongly bound) in contact with CP43, CP26, and CP29; and two more trimers (trimer M, moderately bound) in contact with CP29 and CP24. This complex is generally known as the $C_2S_2M_2$ supercomplex (13). Complexes with smaller antenna sizes have also been described (12).

In addition to limiting the acquisition of structural information, the difficulty of purifying PSII supercomplexes to homogeneity has prevented functional and spectroscopic studies. The available data on light-harvesting processes in PSII were obtained in grana membrane preparations enriched in PSII-LHCII (BBY preparations), which are rather complex and heterogeneous systems.

Most picosecond studies on entire chloroplasts or thylakoid membranes suggested average values for the trapping

Submitted February 17, 2011, and accepted for publication March 30, 2011.

*Correspondence: stefano.caffarri@univmed.fr or Herbert.vanAmerongen@wur.nl

Editor: Leonid S. Brown.

0006-3495/11/05/2094/10 $2.00

doi: 10.1016/j.bpj.2011.03.049

time in PSII in the range of ~300 to ~500 ps (14–16), although later studies on PSII membranes showed average lifetimes on the order of 150 ps (17,18). The exciton/radical-pair-equilibrium (ERPE) model has frequently been used to interpret the kinetics of PSII preparations. In this model, it is assumed that the excitation energy transfer through the antenna to the RC is extremely fast and hardly contributes to the overall charge separation time (19–21). This assumption was criticized or questioned in later studies (1,17,22–24). Broess et al. (18) recently assessed the validity of the ERPE model by obtaining picosecond fluorescence measurements after excitation at different wavelengths and applying a coarse-grained model to determine the excitation migration time to the RC. They concluded that although the excitation energy transfer is slower than was originally assumed in the ERPE model, its contribution to the overall excitation energy trapping time is not a major one (~20–25%) for BBY particles. In the coarse-grained model, it is assumed that PSII has the same organization in BBY particles as it does in supercomplexes (17). However, the modeling can only be approximately correct because the average number of LHCII complexes in the BBY particles is higher than that in the supercomplexes (2.45 vs. 2.0 trimers per RC), the composition and structure of which are used for the modeling. In a recent study (25), the average excitation migration time was found to be substantially larger (~330 ps) for thylakoid membranes of *A. thaliana* when four LHCII trimers per RC were present.

Recently, we were able to isolate homogeneous PSII supercomplexes with different antenna sizes and determine their exact composition and structural organization (26). This offers the possibility to study and model the fluorescence kinetics of PSII preparations, including the outer antenna, in far more detail. In this work, we studied these preparations using picosecond fluorescence spectroscopy, and interpreted the fluorescence decay kinetics using an improved coarse-grained model based on the one presented by Broess et al. (17) to extract excitation- and electron-transfer parameters. We compared the results obtained for different supercomplexes with each other as well as with results previously obtained for core preparations and PSII membranes. Using the newly extracted parameters and the coarse-grained model, we investigated several aspects of PSII functioning, in particular the connectivity between complexes within the $C_2S_2M_2$ supercomplex, the possible connectivity between the supercomplexes and external trimers in the thylakoid membrane, the importance of the PSII dimeric structure, and the relation between the position of an excitation quencher and its efficiency.

MATERIALS AND METHODS

Preparation of PSII supercomplexes

PSII supercomplexes were prepared by solubilizing and fractionating *Arabidopsis* grana membranes according to Caffarri et al. (26). Spectroscopic measurements were performed on freshly prepared PSII particles in the presence of 0.01% or 0.001% α-DM, 10 mM Hepes, pH 7.5.

High-performance liquid chromatography

We used high-performance liquid chromatography for pigment analysis as described previously (27). Pheophytin and β-carotene contents were measured by integrating the signal at 410 nm and 440 nm, respectively.

Time-correlated single-photon counting

Time-correlated single-photon counting measurements were performed at 10°C as described previously (28) with the modification described by Broess et al. (17,18). Measurements were repeated twice for each sample, and the results were nearly identical in all cases. Different preparations could give rise to somewhat different results, but the trends were always the same, i.e., increasing average lifetimes with increasing antenna size and somewhat decreasing lifetimes for lower detergent concentrations.

Coarse-grained model

Modeling of the fluorescence decay was based on a coarse-grained model as described previously (17). The fitting was performed on fluorescence decay curves that were reconstructed from the three fastest components of a four-exponential fit of the original data. The slowest component (~3 ns) with small amplitude is ascribed to some badly connected or totally detached Lhc, and it was not used to reconstruct the decay kinetics. In the coarse-grained model, we used four free parameters: 1), τ_h, the intercomplex excitation hopping time, normalized to one Chl *a* (see below for further explanation of this definition, which differs from previous ones); 2), τ_{CS}, the overall charge separation time in the reaction center, considering six porphyrins per RC; 3), ΔG, the drop in free energy upon primary charge separation; and 4), τ_{RP}, the time for radical pair relaxation (or secondary irreversible charge separation). We set τ_{diss}, the intrinsic excitation dissipation time (excited-state lifetime) in an LHC, to 3200 ps, a typical average lifetime for isolated antenna complexes that can vary somewhat (29). We then fitted the reconstructed decay curves on a time interval of 666 ps (approximately four times the average excited-state lifetime of the PSII supercomplexes) using a set of 37 time points taken according to the equation $X_i = i + X_{i-1}$ ($X_0 = 0$ ps). For samples containing two kinds of particles (B8 and B9), we performed the fitting by summing two curves that described the decay kinetics of each particle weighted by their relative concentration.

The definition of τ_h (and consequently the transfer and adjacency matrices) was modified with respect to previous publications (17,30). In particular, the A_{ij} element for $i \neq j$ (representing the energy transfer step from the complex *j* to the complex *i*) is defined by the value of $-1/n_j$ (where n_j is the number of Chls *a* in the complex *j*). This is different from the previous definition, in which the A_{ij} element was defined as -1 when $n_i \geq n_j$, and $-n_i/n_j$ when $n_i < n_j$ (in an isoenergetic system). We used this modified definition to take into account the entropic factor due to different Chl *a* contents in two adjacent complexes, and consequently to scale the forward and backward energy transfer rates. The entropic factor is also taken into account with the new definition, but now each rate is scaled based on the Chl *a* content of each complex. This prevents the hopping times from being the same for complexes with different Chl contents. It is important to note that with the new definition, the coarse-grained fitting leads to almost the same values for the other three fitting parameters (τ_{CS}, ΔG, and τ_{RP}). In the case of τ_h, the value presented by Broess et al. (18) reflects the average hopping time between complexes, whereas with the new definition it represents a hopping time per Chl *a*, and one can easily calculate the real hopping time by multiplying τ_h with the number of Chls *a* per donor complex. Because the obtained parameters hardly differ between the two models, the previous conclusions remain valid (18). Some other small differences with respect to previous models (17,30) are discussed further below.

The calculation of the initial excitation vector is described in Table S1 and Fig. S1 of the Supporting Material.

RESULTS AND DISCUSSION

PSII supercomplexes with different antenna sizes were purified from grana membranes. The supramolecular organization of the complexes was determined by biochemical and electron microscopy/single-particle analysis (26). The results of these analyses are presented in Fig. 1 in the form of cartoons. The different samples are named after their mobility in a sucrose gradient: Band 8 (B8) contains mainly C_2S supercomplexes (90%) and a small fraction of C_2M complexes (10%). Band 9 (B9) is a mixture (50:50) of C_2S_2 and C_2SM. Band 10 (B10) and band 11 (B11) contain mainly C_2S_2M and $C_2S_2M_2$ complexes, respectively. The $C_2S_2M_2$ particle is the largest supercomplex observed in *A. thaliana* (13), and its structure was previously used to model the fluorescence kinetics of BBY particles (17).

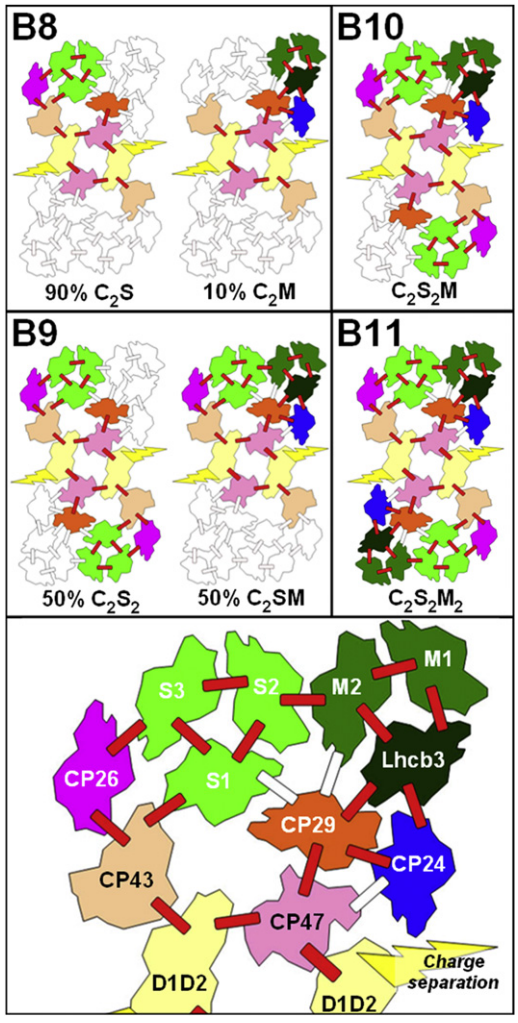

FIGURE 1 Protein composition and supramolecular organization of PSII supercomplexes in the B8, B9, B10, and B11 fractions. PSII connectivity used for the coarse-grained model is shown (*red*, active connections; *white*, inactive connections. The possible importance of these links was tested by switching them on (see text). The major antenna complex, LHCII (*green*), forms trimers that are strongly (S1–S3) or moderately (M1, M2, and Lhcb3) bound (in color in the web version).

Time-resolved fluorescence measurements were performed on the dimeric core complex and on fractions B8, B9, B10, and B11 in solutions containing 0.01% α-DM (as in the sucrose gradient used for the preparation) and 0.001% α-DM. The measurements performed in the presence of 0.001% α-DM were intended to mimic the BBY situation, where detergent is used only to isolate the membrane and is absent in the final preparations that are studied with time-resolved fluorescence (17,18). The results for 0.01% are given in Fig. 2 *A*. As the supercomplexes increase in size, the fluorescence decay becomes progressively slower. The kinetics can be well described by a sum of four exponential decay components in all cases, and the fitting results are given in Table 1 *A*. It should be noted that the fitted components do not necessarily correspond to specific physical processes (17); rather, they serve mainly as an accurate representation of the data and will be used for further analysis below. In all cases, a component of ~3 ns is observed, and its amplitude increases somewhat (from 5% to 8%) with the increasing size of the supercomplex. In principle, this component could be due to some badly connected LHCs, completely disconnected LHCs, free Chl, or closed RCs. However, regardless of its exact origin, this component will be discarded in the analysis presented below, and the average excited-state lifetimes that are listed in Table 1 were calculated without including it.

The fitting results obtained in the presence of 0.001% α-DM are presented in Table 1 *B*. Again, an increase in the size of the complexes leads to a slowing-down of the fluorescence kinetics, and the decay curves can be satisfactorily fitted with the sum of four exponential decay components. For all preparations, the presence of 0.001% α-DM leads to somewhat faster kinetics as compared with 0.01% α-DM. The amplitude of the slowest component is substantially smaller for 0.001% α-DM, being at most ~2%. The average lifetimes for all preparations in both 0.01% α-DM and 0.001% α-DM are plotted versus the number of Chl *a* molecules (Fig. 3) together with the average lifetime obtained for BBY particles (after excitation at 420 nm). On average, these BBY particles contain 2.45 LHCII trimers per reaction center (18), i.e., 226 Chls *a* (+ Pheo) per dimeric RC. It is important to note that at both detergent concentrations, the average excited-state lifetime of the $C_2S_2M_2$ supercomplex (143 ps in 0.001% DM, 158 ps in 0.01% DM) is similar to the BBY average lifetime (154 ps (18)). However, Fig. 3 shows that the results for the BBY complexes are more in line with those obtained from supercomplexes in 0.001% α-DM than those obtained in 0.01% α-DM, suggesting that the detergent is slightly disrupting the packing. When the amount of DM exceeds the critical micelle concentration, PSII is present as isolated complexes, surrounded by detergent (31). Lowering the amount of detergent presumably leads to a tighter packing of the various complexes and thus to faster energy migration. In PSII membranes, the individual supercomplexes are also

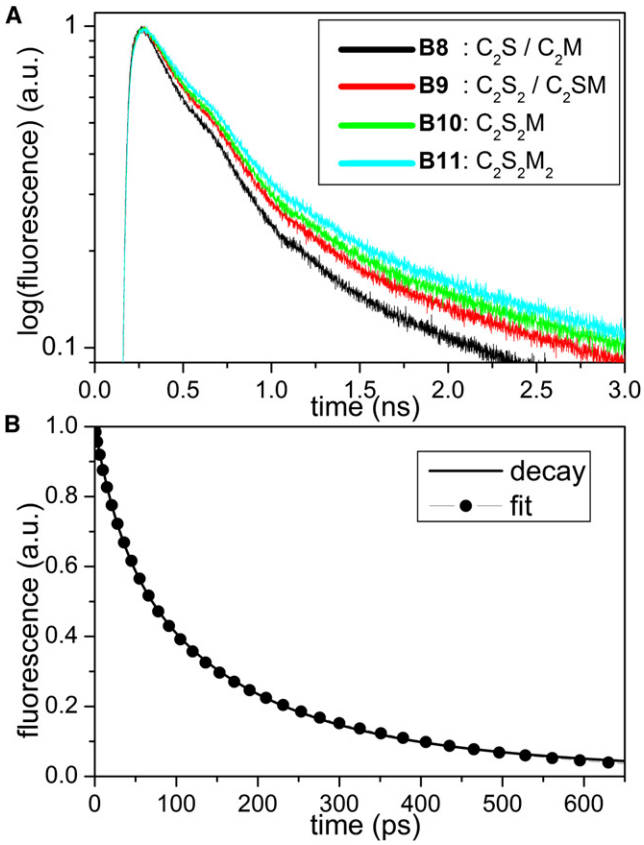

FIGURE 2 (*A*) Fluorescence decay curves of supercomplexes upon 420 nm excitation measured in the presence of 0.01% α-DM and normalized to the maximum value. (*B*) Reconstructed fluorescence decay (*line*) for the B11 sample in 0.01% α-DM using the three main decay components and the best fit using the coarse-grained model (*thin line + dots*) over a time range of 0–666 ps. Fits for the other samples have a similar quality.

closely packed and can even form microcrystalline arrays (13). The protein/lipid ratio in these membranes is extremely high, and a decrease of this ratio also gradually disrupts the packing and energy transfer within PSII (32).

In Fig. 3 it can be seen that there is a nearly linear relationship between the number of Chls of the various complexes and the average excited-state lifetime, but it should be noted that the corresponding linear fits do not pass through the point (0, 0), in contrast to what one might expect (1). As will be discussed below, this means that the excitation trapping performance of a certain supercomplex improves in the presence of additional LHCs.

Coarse-grained modeling of the fluorescence kinetics

We interpreted the fluorescence decay data using a coarse-grained model that was previously conceived to study energy trapping kinetics in grana membranes (17). Here, we slightly modified the original model on the basis of new results regarding PSII organization (26), as shown in Fig. 1. In particular, we removed the energy connection CP24-CP47 because in this region a specific plant core subunit separates CP24 from the core (13,26), and there is no evidence supporting Chl binding in this region. The connection CP24-CP29 was added and the connection between CP29 and trimer M was readjusted such that the monomeric LHCII subunit that was in contact with CP24 (most likely Lhcb3 (26)) is now also in contact with CP29. As explained in the Materials and Methods section, we modified the definition of the transfer matrix and the τ_h-value does not have the same meaning as before (18). In particular, it is no longer the average hopping time between complexes; instead, it is the hopping time per Chl *a*. We calculate the effective hopping time for each connection by multiplying τ_h by the number of Chls *a* per donor complex. Therefore, we also reanalyzed the previous results (18) with the new model.

The best least-squares fits of the fluorescence kinetics obtained with the coarse-grained model are shown in Table 2 for complexes in 0.01% and 0.001% α-DM together with the fitting results for BBY membranes. Fig. 2 *B* shows, as an example, the reconstructed decay for the B11 sample in 0.01% α-DM and its fit.

The value for the drop in free energy upon primary charge separation (ΔG) is in rather good agreement with the fitting results for BBY membranes (18), particularly for the largest complexes in the presence of 0.001% DM. The secondary charge separation time (τ_{RP}) is similar to the value found by Broess et al. (18) but somewhat larger than the refitted value.

We note that faster energy transfer (i.e., smaller τ_h) is found more often in the 0.001% α-DM samples than in the 0.01% α-DM samples. This supports the above suggestion that detergent removal may lead to better connectivity between the individual subunits in the supercomplexes.

With regard to the hopping time (τ_h) and the charge separation time (τ_{CS}), we would like to emphasize that a gradual decrease of both time constants occurs with increasing antenna size. Moreover, the fitted parameters differ to some extent from the parameters obtained for the BBY particles. These two points will be discussed in detail further below.

Before we begin to discuss these observations, it is important to point out that one cannot independently determine τ_h and τ_{CS}. There is an inverse relationship between these parameters, i.e., by increasing one and decreasing the other, one can still obtain a relatively good description of the data (17). Broess et al. (18) resolved this ambiguity by using two excitation wavelengths that excited Chls *a* and *b* to different extents. However, this approach did not appear to be applicable for the complexes studied here, most likely because of the presence of a small and variable amount of badly connected Chl *b* molecules, which are probably responsible for the longer decay times observed upon excitation at 483 nm (~10 ps more than expected).

TABLE 1 Fluorescence decay fitting results of samples in 0.01% α-DM (*A*) and 0.001% α-DM (*B*)

(*A*)

Core		B8		B9		B10		B11	
τ (*ps*)	*A*	τ (*ps*)	*A*	τ (*ps*)	*A*	τ (*ps*)	*A*	τ (*ps*)	*A*
28	50.4%	25	32.3%	29	30.6%	30	26.4%	31	26.3%
104	32.0%	112	49.0%	127	48.3%	128	51.3%	137	49.5%
413	14.1%	393	13.8%	421	14.6%	421	15.1%	439	15.7%
2209	3.5%	2989	5.0%	3201	6.5%	3256	7.5%	3215	8.5%
τAV (ps)	109	τAV (ps)	123	τAV (ps)	141	τAV (ps)	148	τAV (ps)	158

(*B*)

Core		B8		B9		B10		B11	
τ (*ps*)	*A*	τ (*ps*)	*A*	τ (*ps*)	*A*	τ (*ps*)	*A*	τ (*ps*)	*A*
21	59.8%	24	38.8%	25	35.5%	25	36.1%	27	22.8%
94	29.2%	108	49.0%	114	49.9%	120	49.0%	120	56.9%
378	9.3%	382	10.4%	377	12.5%	379	12.8%	377	16.9%
1717	1.7%	2223	1.8%	2262	2.1%	2335	2.1%	2348	3.4%
τAV (ps)	77	τAV (ps)	104	τAV (ps)	115	τAV (ps)	119	τAV (ps)	143

Average excited-state lifetimes are calculated from the first three lifetimes according to $\tau_{AV} = \sum_{i=1-3} \tau_i \cdot A_i / \sum A_i$.

Kinetic parameters and antenna size

Both τ_h and τ_{CS} decrease with an increase in antenna size, with the only exception being the step from B10 to B11 in 0.001% α-DM. If it is assumed that the charge separation parameters remain the same, the hopping rate speeds up even more with increasing antenna size (Table S1).

To investigate this variation in more detail, we fitted and fixed the kinetics of a certain complex (e.g., B10 in 0.01% α-DM) and then added the extra antenna complexes present in the next supercomplex (i.e., B11 with one more CP24 and LHCII trimer) and calculated which additional transfer rates were needed to correctly describe the observed kinetics. Even when infinitely fast hopping times were assumed for transfer from/to these additional complexes, the modeled kinetics was slower than the measured one. This means that excitation energy transfer and/or charge separation (in the B10 subpart of B11) should become faster. The same trend can be observed for all complexes except when going from B10 to B11 in 0.001% α-DM. This means that the electron transfer and/or excitation transfer becomes relatively slower during the gradual loss of antennae. Biochemical data show that some structural changes occur in the core complex: as the Lhc antenna decreases in size, the core subunit PsbQ (OEE17) is gradually lost (26). We also found that the β-carotene/pheophytin ratio is higher in $C_2S_2M_2$ particles than in the purified core complex, indicating the lack of one β-carotene in the latter. However, at this point, we cannot conclude whether these structural changes are related to the changes in the trapping process.

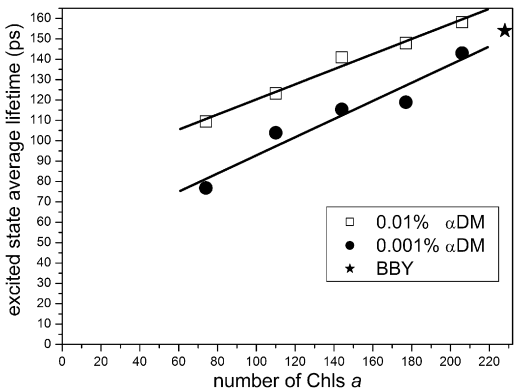

FIGURE 3 Average excited-state lifetimes versus number of Chl *a* molecules per complex in each fraction in 0.01% and 0.001% α-DM. The lines represent linear fits. The star indicates the average excited-state lifetime of BBY particles (420 nm excitation (18)).

Comparison of kinetic parameters with previous results on cores

It is relevant to compare our results with previous results obtained from various core preparations. The average fluorescence lifetime we obtained here (109 ps) is similar to that obtained by Tumino and co-workers (33) in core preparations from spinach (104 ps). However, as noted above, the trapping kinetics of the core speeds up considerably when the core is embedded in the supercomplexes. When the parameters obtained by averaging the fitting results for B10 and B11 (i.e., the most intact supercomplexes) in 0.01 and 0.001% α-DM (τ_h = 0.75 ps, τ_{CS} = 2.50 ps, τ_{RP} = 150 ps, and ΔG = 715 cm^{-1}) are used, the average lifetime of the core alone becomes significantly shorter (~50 ps) and resembles more the result obtained by Miloslavina et al. (34) in cores from cyanobacteria (~60 ps), which are not embedded in supercomplexes in vivo. The hopping time for excitation energy transfer from CP47 and CP43 to the

TABLE 2 Results of fitting obtained using the coarse-grained model with all four parameters being free

	0.01% α-DM					0.01% α-DM					
	Core	B8	B9	B10	B11	Core	B8	B9	B10	B11	BBY refit
τh (ps)	1.8	1.4	0.9	0.9	0.7	1.2	1.1	0.8	0.6	0.8	0.7
τCS (ps)	5.2	3.3	3.2	2.8	2.7	3.6	2.9	2.6	2.1	2.4	4.1
τRP (ps)	191	202	173	167	151	152	177	154	132	143	113
ΔG (cm^{-1})	596	741	697	726	706	620	742	711	691	733	764

Fitting results are also shown for BBY data previously obtained (18) with the coarse-grained model presented here.

RC becomes 12.8 ps and 10.5 ps, respectively, with a backward transfer time of 4.5 ps in both cases. Also, these values are rather similar to those found for the cyanobacterial core (forward 11 ps and 8 ps, and backward 6.4 ps and 4.3 ps, respectively) (34). Furthermore, the drops in free energy observed in our one-step model and the two-step radical pair model of Miloslavina et al. (34) are comparable (~720 cm^{-1} and 860 cm^{-1} (107 meV), respectively).

Within the context of our coarse-grained model, the migration time (τ_{mig}, the average time it takes for an excitation created somewhere in PSII to reach the RC (17,18)) accounts for only 16% of the overall trapping time (τ_{av}), both when the core is extrapolated from the $C_2S_2M_2$ complex and when it is purified. However, far longer migration times have also been proposed in the literature. For instance, Raszewski and Renger (35) proposed the following transfer values: 50/41 ps for CP47/43→RC, and 16/22 ps for RC→CP47/CP43. We tested the same values within our model for the largest PSII supercomplexes (C_2S_2M and $C_2S_2M_2$), and tried to adapt the other parameters to obtain a good description of the observed fluorescence kinetics. However, unreasonably fast effective hopping times between different complexes (far below 1 ps) and extremely fast charge separation times of ~0.5 ps for an equilibrated RC are needed to obtain the correct average lifetime, and the quality of the fits is poor. In conclusion, slow energy transfer in the core complex, as proposed by Raszewski and Renger (35), is not in agreement with the fast kinetics of the largest PSII-LHCII supercomplexes. In a very recent study, van der Weij de Wit et al. (36) modeled the fluorescence kinetics of core preparations from *Thermosynechococcus elongatus* with excitation energy transfer kinetics that were intermediate between those mentioned previously (34,35).

Supercomplexes versus BBY

The kinetic parameters obtained from the coarse-grained modeling of the largest PSII particles (average of B10 and B11) are not completely identical to those obtained for PSII membranes (Table 2). Both systems—supercomplexes and PSII membrane preparations (BBY)—have advantages and drawbacks. Membranes constitute a virtually intact system, but their composition and organization are somewhat heterogeneous and not completely known, particularly regarding the additional LHCII trimers and the contacts between the stacked grana membranes. On the other hand PSII particles in solution have a well-known structural organization, but the purification protocol requires a detergent treatment of the membranes that can partially impair the PSII structure and kinetic behavior.

In conclusion, some uncertainty remains concerning the best parameters to use within the context of the coarse-grained model. However, because the differences are relatively small and do not significantly influence the subsequent modeling results, we chose to use the average values obtained for the most intact supercomplexes (B10 and B11), hereafter called the standard parameter set ($\tau_h = 0.75$ ps, $\tau_{CS} = 2.5$ ps, $\tau_{RP} = 150$ ps, and $\Delta G = 715$ cm^{-1}), to investigate the following topics: connectivity in the $C_2S_2M_2$ supercomplex, possible connectivity of extra trimers, importance of the PSII dimeric structure, and exciton quenching in PSII.

Connectivity between complexes within the supercomplex in relation to light harvesting

In our approach, the overall trapping time (or average excited-state lifetime τ_{av}) is the sum of τ_{mig} and τ_{trap} ($\tau_{av} = \tau_{trap}+\tau_{mig}$). τ_{trap} is the charge separation time when the excitation is spatially/thermodynamically equilibrated over PSII and is proportional to the Chl content. When the standard parameter set is used, the average lifetime (τ_{av}) and migration time (τ_{mig}) for the $C_2S_2M_2$ particle are calculated to be 146 ps and 42 ps, respectively. In Fig. S2 we illustrate how the average excited-state lifetime changes when a connection between two complexes is removed or added (both symmetrical connections are changed at the same time). The changes in the average lifetime are entirely due to changes in the migration time. Removing the connection between CP43 and D1/D2 leads to an increase of the average excited-state lifetime from 146 ps to 236 ps, and eliminating the connection between CP29 and CP47 leads to an increase from 146 ps to 187 ps. However, most of the other connections can easily be removed without substantially affecting the overall trapping time, reflecting the robustness of the light-harvesting system.

Connectivity of additional trimers

Under low- to medium-light growth conditions, the thylakoid membrane contains up to four more LHCII trimers per

dimeric PSII as compared with the $C_2S_2M_2$ complex and the average PSII lifetime is ~330 ps (25), more than double the value found for $C_2S_2M_2$. Using our standard parameter set, a value of $\tau_{trap} = 155$ ps is expected for a complex containing these extra trimers, meaning that τ_{mig} should be ~175 ps, which is similar to the 150 ps calculated previously (25).

Using a simple model (extra trimers are connected to each other, and each trimer has one connection to PSII; Fig. S3) and taking the hopping time from the extra trimers to be the same as in the supercomplexes (0.75 ps), we calculate the total average lifetime to be 237 ps, far below the experimental value of 330 ps. The hopping time from the extra trimers to the $C_2S_2M_2$ complex must be 20 times slower to obtain an overall trapping time of 330 ps. Of course, different organizations/connections lead to different values: in the case of a very low number of connections (i.e., only one connection per pair of external trimers), the hopping time becomes faster but it will still be ~10 times slower than it would be for internal trimers. In any case, the migration time from external LHCII (calculated by setting the entire initial excitation on a single complex in the model) is ~400 ps, which is far slower than that from internal Lhc antennae (60–90 ps) but still fast enough for efficient photosynthesis. Note that the parameters obtained in this study are not in agreement with the work of Barter et al. (37), who concluded that charge separation in PSII is trap-limited regardless of the size of the antenna system (for further discussion of this issue, see Croce and van Amerongen (9)).

Consequences of dimeric PSII organization

Although under certain conditions PSII may exist as monomers (38), in most cases it is organized as dimers. If one PSII RC is closed, excitations can still be used by the other RC in a dimeric PSII structure. With our standard parameter set, it is possible to estimate the corresponding efficiency. It is important to remember that although a closed RC can perform charge separation, the radical pair will quickly recombine, which may yield fluorescence owing to repopulation of the excited state (39). The amount of energy that returns into the system as excitation is calculated based on in vivo measurements on PSII with closed RCs. To simulate a closed RC, we increased τ_{CS} to obtain a fivefold increase of the PSII fluorescence yield to reproduce the fluorescence variations measured in vivo (F_m and F_0, fluorescence in the presence of closed and open RCs, respectively (30)). Using the extended model representing the in vivo situation (Fig. S3), we calculate an increase of τ_{CS} from 2.5 to 124 ps.

The competition among three processes must be calculated: 1), trapping by open RC (photochemistry with rate constant K_{phot}); 2), trapping by a closed RC (wasted energy, $K_{RC\text{-}diss}$); and 3), the normal dissipative route (K_{diss}, fixed in the model at $(3.2\ ns)^{-1}$). The photochemistry yield can then be calculated via $K_{phot}/\Sigma K$ (where ΣK is the sum of all processes). With two open RCs, K_{phot} is the inverse of τ_{av} of the system calculated in the absence of the dissipative route and corresponds to $(377\ ps)^{-1}$. This leads to a PSII efficiency of 89%. In presence of only one open RC, K_{phot} is calculated to $(590\ ps)^{-1}$ (after eliminating the second RC by setting its τ_{CS} to infinite). In the same way, the rate of trapping by a closed RC ($K_{RC\text{-}diss}$) is calculated to be $(2760\ ps)^{-1}$. The photochemical efficiency $K_{phot}/(K_{phot} + K_{RC\text{-}diss} + K_{diss})$ of a dimeric PSII with one closed RC is then 78%. This should be compared with an efficiency of ~45% in the case of two monomers (one being unable to perform photosynthesis, and one having an efficiency of 89%). This indicates that a dimeric conformation increases light-harvesting utilization by >70% in the presence of one closed RC, which is an important property for PSII given its slow turnover.

It should be noted that the PSII photosynthetic efficiency with open RCs calculated here is higher than what is found with pulse-amplitude-modulated (PAM) fluorescence measurements (~83%). A discussion about possible reasons for this discrepancy is presented in Appendix S1.

Excitonic quenching simulations

Finally, we analyzed the influence of one or more quenching sites in PSII, using an approach similar to that of Valkunas et al. (30) with modified parameters, by trying to simulate possible nonphotochemical quenching (NPQ) scenarios. In short, by setting a quencher in any of the Lhc proteins, we can calculate the theoretically best location for a quencher. Note that the quencher identity is still not clear, because different studies have suggested that the quencher forms in either the major light harvesting complexes LHCII (40) or the minor antennae (41), or possibly in both (42). We performed the analysis in the presence of closed RCs, i.e., in the situation where the quenching is most useful, which is also the same condition used for NPQ determination by the PAM saturating flash technique (43).

Using the coarse-grained model built for in vivo kinetics (i.e., with extra trimers) and taking one quencher with three possible quenching times τ_{npq} or inverse quenching rates (50 ps, 5 ps, and 0.5 ps), we found that the position of the best quencher is not unique. It is important to mention that the quenching time corresponds to the value when energy is on a particular quenched complex, and is not the time constant for energy dissipation when the excitation is on the quencher itself (e.g., a Chl-carotenoid couple or a Chl-Chl dimer). The latter time is obtained by dividing the former time by the entropic factor, i.e., the number of Chls *a* in the Lhc complex that harbors the quenching site (with the approximation of isoenergetic pigments). In the case of a relatively slow quenching process (50 ps), LHCII monomers in the S and M trimers would be the best quenchers, but in the case of extremely fast quenching (0.5 ps), CP29 would be the best (Table 3). Of interest, in all cases external trimers are the less efficient quenchers of PSII excitation.

TABLE 3 Average excited-state lifetime (in picoseconds) of PSII with closed RCs in the presence of one or two quenching sites on the indicated antenna

	One site			Two sites			
τNPQ→	50 ps	5 ps	0.5 ps	50 ps	5 ps	0.5 ps	
CP29	1079	451	**304**	808	284	193	Minor antennae
CP26	1035	469	350	754	278	201	
CP24	1144	520	363	878	320	217	
Lhcb3	**978**	**418**	307	696	245	175	LHCII-M
M1	984	448	344	696	252	184	
M2	978	424	315	**692**	240	171	
S1	982	426	316	699	247	178	LHCII-S
S2	978	423	313	693	**239**	**169**	
S3	980	428	319	694	242	172	
LM1	1080	823	784	714	398	354	Extra LHCII L–M
LM2	1085	834	797	719	409	366	
LM3	1077	819	779	709	390	346	
LS1	1080	823	784	714	398	354	Extra LHCII L–S
LS2	1077	818	779	709	390	346	
LS3	1085	834	797	719	408	366	

Best quenchers for a particular quenching rate are shown in bold. See Fig. 1 and Fig. S3 for the nomenclature and position of each Lhc complex.

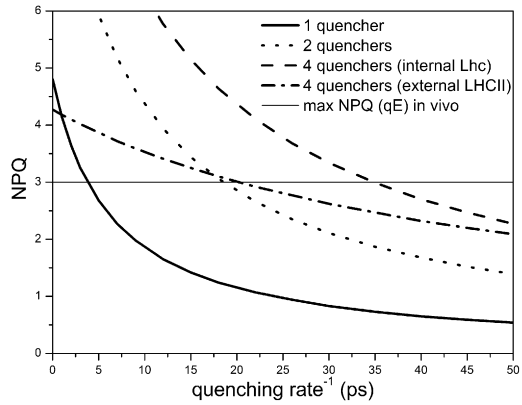

FIGURE 4 Effect on NPQ of the number, position, and rate of the quenchers. Quenchers were set as follows: one quencher on the best single quencher (CP29); two quenchers on the best double quencher (LHCII monomer, termed S2 in Fig. 1); four quenchers simultaneously on the previous four (internal Lhc); or the four extra trimers (*dash-dotted line*). An NPQ value of 3 (*horizontal line*) indicates a typical value for efficient quenching in vivo.

This outcome differs from that reported by Valkunas et al. (30), who also concluded that external trimers were very good quenchers in all cases. However, it should be noted that in our model, four extra trimers were added per $C_2S_2M_2$ supercomplex (as found in thylakoids) instead of 12 (30). This excessive number was necessary to reproduce in vivo kinetics, because extra trimers were connected with the same transfer rates as the rest of PSII. Here we have used a more realistic description with the right stoichiometry and a decreased connectivity of the extra trimers.

The fact that in our simulations CP29 was the best quencher when a very fast quenching process was assumed (also in the case of $C_2S_2M_2$ particles; not shown) mainly reflects the different connectivity that was used with respect to the study by Valkunas et al. (30). The removal in our model of the link CP24-core led to an increased energy flow through CP29. When instead of one quencher per PSII dimer, two quenchers were placed on two identical symmetry-related complexes, the LHCIIs belonging to the S and M trimers became the most efficient quenchers for any tested quenching rate (Table 3), and a similar observation was made for the $C_2S_2M_2$ complex (not shown).

Using the classical PAM equation $(Fm - Fm')/Fm'$ to calculate NPQ rewritten as $(\tau_{av\text{-}RCC} - \tau_{av\text{-}NPQ})/\tau_{av\text{-}NPQ}$ (where $\tau_{av\text{-}RCC}$ is the PSII average lifetime with closed RCs, and $\tau_{av\text{-}NPQ}$ is the average lifetime with closed RC and active quenching), we can plot NPQ versus the quenching rate in the case of one or more sites.

Assuming that an efficient quencher induces an amount of NPQ = 3 (Fig. 4, *horizontal line*; NPQ can be higher in vivo, but other components, such as photoinhibition and state transition, are also present (44)), it can be observed that the number and position of the quenchers have an important effect on the excitation dissipation. In the case of a single site, efficient energy dissipation requires a fast quencher, on the order of 3–4 ps. However, in the presence of two quenchers per PSII, efficient energy dissipation can be obtained with far slower quenchers, on the order of ~20 ps. With four quenchers per dimeric core, relatively slow quenchers (35 ps) would still be efficient for thermal dissipation. In the case of four quenchers located in the external trimers (one quencher in each trimer), the quenchers require quenching times on the order of 20 ps. In this case, the quenching rate has a smaller effect on NPQ efficiency, as judged by the less-steep slope of the curve associated to an externally located quencher (Fig. 4). Of interest, for an NPQ value of ~3, similar results (apart from the quenchers on the L trimers) are obtained using the $C_2S_2M_2$ complex (not shown).

An important aspect of the current analysis is the fact the location of the quencher has minor importance in terms of the quenching efficiency (variation at most 30%, not considering the external trimers). In addition, the migration times required to reach each site (calculated as the average lifetime in the presence of $\tau_{npq} \rightarrow 0$) are similar and much more rapid than the average lifetime of a PSII with closed RCs (in our simulation ~300 ps versus 1650 ps, respectively). Thus, a relatively small increase in the quenching rate can compensate for a less advantageous position. Therefore, we propose that PSII does not need a particular optimal position for energy quenching; rather, the location of the quencher is more likely determined by the possibility of creating a quencher in that particular position (e.g., by interacting with the PsbS protein).

CONCLUSIONS

Fluorescence decay kinetics and biochemical analysis (singular/not plural) of plant PSII supercomplexes with

different antenna sizes indicate that the antenna system is important for the integrity and connectivity of the core and supercomplexes.

The average excited-state lifetime of the purified $C_2S_2M_2$ supercomplex is ~150 ps.

The results from coarse-grained modeling suggest that:

1. Two connections (CP43-RC and CP29-CP47) have a major role in transferring excitation energy inside PSII, whereas the other connections are to some extent redundant, making the light-harvesting system robust.
2. Loosely bound LHCII trimers present in thylakoids and located externally to the $C_2S_2M_2$ supercomplexes possess slow connections to PSII (at least ~10 times slower than the S and M trimers).
3. The dimeric conformation of PSII allows >70% more efficient photochemistry in the presence of one closed RC compared with two PSII monomers with one closed RC.

Modeling of nonphotochemical quenching indicates that efficient quenchers at low concentration are probably located inside the $C_2S_2M_2$ complex. However, considering the relatively small differences, each antenna position may be a good location for quenching. Quenchers can be efficient in the external trimers only when they are present in high concentrations.

SUPPORTING MATERIAL

Two tables, three figures, and an appendix are available at http://www.biophysj.org/biophysj/supplemental/S0006-3495(11)00407-3.

This work was performed as part of a research program of the Stichting voor Fundamenteel Onderzoek der Materie, which is financially supported by the Nederlandse Organisatie voor Wetenschappelijk Onderzoek (NWO). The work in Groningen was financed by the Earth and Life Science Division of the NWO via a Vidi grant (to R.C.). S.C. received a visitor grant from the NWO and the Partenariats Hubert Curien (Van Gogh).

REFERENCES

1. van Amerongen, H., and J. P. Dekker. 2003. Light-harvesting in Photosystem II. *In* Light-Harvesting Antennas in Photosynthesis. B. R. Green and W. W. Parson, editors. Kluwer Academic Publishers, Dordrecht. 219–251.
2. Guskov, A., A. Gabdulkhakov, …, A. Zouni. 2010. Recent progress in the crystallographic studies of photosystem II. *ChemPhysChem.* 11:1160–1171.
3. Guskov, A., J. Kern, …, W. Saenger. 2009. Cyanobacterial photosystem II at 2.9-A resolution and the role of quinones, lipids, channels and chloride. *Nat. Struct. Mol. Biol.* 16:334–342.
4. Shi, L. X., and W. P. Schröder. 2004. The low molecular mass subunits of the photosynthetic supracomplex, Photosystem II. *Biochim. Biophys. Acta.* 1608:75–96.
5. Jansson, S. 1999. A guide to the Lhc genes and their relatives in *Arabidopsis*. *Trends Plant Sci.* 4:236–240.
6. Caffarri, S., R. Croce, …, R. Bassi. 2004. A look within LHCII: differential analysis of the Lhcb1-3 complexes building the major trimeric antenna complex of higher-plant photosynthesis. *Biochemistry.* 43:9467–9476.
7. Liu, Z., H. Yan, …, W. Chang. 2004. Crystal structure of spinach major light-harvesting complex at 2.72 A resolution. *Nature.* 428:287–292.
8. Sandonà, D., R. Croce, …, R. Bassi. 1998. Higher plants light harvesting proteins. Structure and function as revealed by mutation analysis of either protein or chromophore moieties. *Biochim. Biophys. Acta.* 1365:207–214.
9. Croce, R., and H. van Amerongen. 2011. Light-harvesting and structural organization of Photosystem II: from individual complexes to thylakoid membrane. *J. Photochem. Photobiol. B*. 10.1016/j.jphotobiol.2011.02.015.
10. Anderson, J. M., and B. Andersson. 1988. The dynamic photosynthetic membrane and regulation of solar energy conversion. *Trends Biochem. Sci.* 13:351–355.
11. Boekema, E. J., H. van Roon, …, J. P. Dekker. 1999. Multiple types of association of photosystem II and its light-harvesting antenna in partially solubilized Photosystem II membranes. *Biochemistry.* 38:2233–2239.
12. Yakushevska, A. E., P. E. Jensen, …, J. P. Dekker. 2001. Supermolecular organization of Photosystem II and its associated light-harvesting antenna in *Arabidopsis thaliana*. *Eur. J. Biochem.* 268:6020–6028.
13. Dekker, J. P., and E. J. Boekema. 2005. Supramolecular organization of thylakoid membrane proteins in green plants. *Biochim. Biophys. Acta.* 1706:12–39.
14. Roelofs, T. A., C. H. Lee, and A. R. Holzwarth. 1992. Global target analysis of picosecond chlorophyll fluorescence kinetics from pea chloroplasts: a new approach to the characterization of the primary processes in photosystem II α- and β-units. *Biophys. J.* 61:1147–1163.
15. Gilmore, A. M., T. L. Hazlett, …, Govindjee. 1996. Photosystem II chlorophyll a fluorescence lifetimes and intensity are independent of the antenna size differences between barley wild-type and chlorina mutants: photochemical quenching and xanthophyll cycle-dependent nonphotochemical quenching of fluorescence. *Photosynth. Res.* 48:171–187.
16. Vasil'ev, S., S. Wiebe, and D. Bruce. 1998. Non-photochemical quenching of chlorophyll fluorescence in photosynthesis. 5-hydroxy-1,4-naphthoquinone in spinach thylakoids as a model for antenna based quenching mechanisms. *Biochim. Biophys. Acta.* 1363:147–156.
17. Broess, K., G. Trinkunas, …, H. van Amerongen. 2006. Excitation energy transfer and charge separation in photosystem II membranes revisited. *Biophys. J.* 91:3776–3786.
18. Broess, K., G. Trinkunas, A. van Hoek, R. Croce, and H. van Amerongen. 2008. Determination of the excitation migration time in Photosystem II—consequences for the membrane organization and charge separation parameters. *Biochim. Biophys. Acta.* 1777:404–409.
19. Schatz, G. H., H. Brock, and A. R. Holzwarth. 1987. Picosecond kinetics of fluorescence and absorbance changes in photosystem II particles excited at low photon density. *Proc. Natl. Acad. Sci. USA.* 84:8414–8418.
20. Schatz, G. H., H. Brock, and A. R. Holzwarth. 1988. A kinetic and energetic model for the primary processes in photosystem II. *Biophys. J.* 54:397–405.
21. van Grondelle, R. 1985. Excitation energy transfer, trapping and annihilation in photosynthetic systems. *Biochim. Biophys. Acta.* 811: 147–195.
22. Barzda, V., V. Gulbinas, …, L. Valkunas. 2001. Singlet-singlet annihilation kinetics in aggregates and trimers of LHCII. *Biophys. J.* 80:2409–2421.
23. van Amerongen, H., and R. van Grondelle. 2001. Understanding the energy transfer function of LHCII, the major light-harvesting complex of green plants. *J. Phys. Chem. B.* 105:604–617.
24. Jennings, R. C., G. Elli, …, G. Zucchelli. 2000. Selective quenching of the fluorescence of core chlorophyll-protein complexes by photochemistry indicates that Photosystem II is partly diffusion limited. *Photosynth. Res.* 66:225–233.

25. van Oort, B., M. Alberts, …, H. van Amerongen. 2010. Effect of antenna-depletion in Photosystem II on excitation energy transfer in *Arabidopsis thaliana*. *Biophys. J.* 98:922–931.

26. Caffarri, S., R. Kouril, …, R. Croce. 2009. Functional architecture of higher plant Photosystem II supercomplexes. *EMBO J.* 28:3052–3063.

27. Campoli, C., S. Caffarri, …, C. Crosatti. 2009. Parallel pigment and transcriptomic analysis of four barley albina and xantha mutants reveals the complex network of the chloroplast-dependent metabolism. *Plant Mol. Biol.* 71:173–191.

28. Somsen, O. J. G., V. A. Hoek, and H. van Amerongen. 2005. Fluorescence quenching of 2-aminopurine in dinucleotides. *Chem. Phys. Lett.* 402:61–65.

29. Palacios, M. A., F. L. de Weerd, …, H. van Amerongen. 2002. Superradiance and exciton (de)localization in light-harvesting complex II from green plants? *J. Phys. Chem. B.* 106:5782–5787.

30. Valkunas, L., G. Trinkunas, …, A. V. Ruban. 2009. Modeling of exciton quenching in Photosystem II. *Phys. Chem. Chem. Phys.* 11:7576–7584.

31. Folea, I. M., P. Zhang, …, E. J. Boekema. 2008. Domain organization of Photosystem II in membranes of the cyanobacterium Synechocystis PCC6803 investigated by electron microscopy. *FEBS Lett.* 582:1749–1754.

32. Haferkamp, S., W. Haase, …, H. Kirchhoff. 2010. Efficient light harvesting by photosystem II requires an optimized protein packing density in Grana thylakoids. *J. Biol. Chem.* 285:17020–17028.

33. Tumino, G., A. P. Casazza, …, R. C. Jennings. 2008. Fluorescence lifetime spectrum of the plant photosystem II core complex: photochemistry does not induce specific reaction center quenching. *Biochemistry.* 47:10449–10457.

34. Miloslavina, Y., M. Szczepaniak, …, A. R. Holzwarth. 2006. Charge separation kinetics in intact photosystem II core particles is trap-limited. A picosecond fluorescence study. *Biochemistry.* 45:2436–2442.

35. Raszewski, G., and T. Renger. 2008. Light harvesting in photosystem II core complexes is limited by the transfer to the trap: can the core complex turn into a photoprotective mode? *J. Am. Chem. Soc.* 130:4431–4446.

36. van der Weij de Wit, C. D., J. P. Dekker, …, I. H. van Stokkum. 2011. Charge separation is virtually irreversible in Photosystem II core complexes with oxidized primary quinone acceptor. *J. Phys. Chem. A*. 10.1021/jp1083746.

37. Barter, L. M., M. Bianchietti, …, D. R. Klug. 2001. Relationship between excitation energy transfer, trapping, and antenna size in photosystem II. *Biochemistry.* 40:4026–4034.

38. Takahashi, T., N. Inoue-Kashino, …, K. Satoh. 2009. Photosystem II complex *in vivo* is a monomer. *J. Biol. Chem.* 284:15598–15606.

39. van Mieghem, F., K. Brettel, …, E. Schlodder. 1995. Charge recombination reactions in photosystem II. I. Yields, recombination pathways, and kinetics of the primary pair. *Biochemistry.* 34:4798–4813.

40. Ruban, A. V., R. Berera, …, R. van Grondelle. 2007. Identification of a mechanism of photoprotective energy dissipation in higher plants. *Nature.* 450:575–578.

41. Avenson, T. J., T. K. Ahn, …, G. R. Fleming. 2008. Zeaxanthin radical cation formation in minor light-harvesting complexes of higher plant antenna. *J. Biol. Chem.* 283:3550–3558.

42. Mozzo, M., F. Passarini, …, R. Croce. 2008. Photoprotection in higher plants: the putative quenching site is conserved in all outer light-harvesting complexes of Photosystem II. *Biochim. Biophys. Acta.* 1777:1263–1267.

43. Schreiber, U., U. Schliwa, and W. Bilger. 1986. Continuous recording of photochemical and non-photochemical chlorophyll fluorescence quenching with a new type of modulation fluorometer. *Photosynth. Res.* 10:51–62.

44. Horton, P., A. V. Ruban, and R. G. Walters. 1996. Regulation of light harvesting in green plants. *Annu. Rev. Plant Physiol. Plant Mol. Biol.* 47:655–684.